Journal of Alloys and Compounds 604 (2014) 94–99

Contents lists available at ScienceDirect

Journal of Alloys and Compounds

journal homepage: www.elsevier.com/locate/jalcom

Preparation and structural evolution of Mo/SiO_x protective coating on $CoSb_3$-based filled skutterudite thermoelectric material

Xugui Xia, Xiangyang Huang *, Xiaoya Li, Ming Gu, Pengfei Qiu, Jincheng Liao, Yunshan Tang, Shengqiang Bai, Lidong Chen

CAS Key Laboratory of Materials for Energy Conversion, Shanghai Institute of Ceramics, Chinese Academy of Sciences, 1295 Dingxi Road, Shanghai 200050, China

ARTICLE INFO

Article history:
Received 13 January 2014
Received in revised form 7 March 2014
Accepted 10 March 2014
Available online 26 March 2014

Keywords:
Protective coating
$CoSb_3$-based filled skutterudite
Sb sublimation
Thermoelectric device
Aging

ABSTRACT

A Mo/SiO_x multilayer film was deposited on a $Ce_{0.9}Fe_3CoSb_{12}$ skutterudite surface as a protective coating by magnetron sputtering. A thermal aging test was conducted under vacuum at 823–923 K, and the microstructural evolution of the multilayer film and the effects of the protective coating on the suppression of Sb sublimation were investigated. The as-prepared Mo layer is crystallized in a body-centered cubic structure with preferred orientation of the (1 1 0) plane parallel to the substrate, whereas the SiO_x layer is amorphous. The formation of a Mo_3Sb_7 interlayer between the skutterudite and coating was observed after the high temperature thermal aging that enhanced the adhesion between the coating and the skutterudite. The Mo_3Sb_7 layer is chemically stable at high temperatures; therefore, it blocks the further diffusion of Mo and Sb on the boundary. The Mo_3Sb_7/Mo/SiO_x multilayer coating can effectively suppress Sb sublimation, enabling high temperature applications of the $CoSb_3$-based thermoelectric device.

1. Introduction

The use of thermoelectric (TE) devices can enable the direct conversion between heat and electrical energy and provide an effective way to recover low-grade heat energy such as industrial waste heat, geothermal energy, solar heat, and automobile exhaust heat. TE technology also has irreplaceable applications including space or other special power sources. The energy conversion efficiency of TE devices depends critically on the performance of TE materials and operation temperature. Many state-of-the-art TE materials have been developed, such as Bi_2Te_3-based alloy, PbTe, $CoSb_3$-based filled skutterudites (SKDs), Zn_4Sb_3, clathrates, $FeSi_2$, and SiGe [1–17]. Among them, $CoSb_3$-based filled SKDs are considered promising materials for power generation in the intermediate temperature range (room temperature to 900 K) for harvesting industrial waste heat and the heat energy of automobile exhaust gases because of their high TE performance in the intermediate temperature range. However, a recent study revealed that $CoSb_3$-based SKDs undergo oxidation and decomposition at temperatures >673 K [18–25], much lower than the peritectic temperature of $CoSb_3$ or $CoSb_3$-based filled SKDs. The decomposition mainly comes from the sublimation of antimony, which will degrade their TE properties and decrease TE device durability. For the practical application of SKD-based TE devices, the development of a feasible technique to suppress sublimation of the volatile antimony from the legs near the hot junction over time in a multi-year operation is important.

There is a similar issue with the sublimation of germanium from SiGe unicouples, which have been successfully used in radioisotope thermoelectric generators (RTGs) during the past four decades [26,27]. The sublimation of germanium has been satisfactorily managed using thin Si_3N_4 coatings. Silica-based composite protective coatings have been fabricated to suppress the sublimation of antimony [28]. A thin metallic coating developed at the Jet Propulsion Laboratory was shown to significantly reduce antimony loss in high-temperature tests [29–31]. Furthermore, a number of tests using SKD-based unicouples (SKUs) with and without coatings have been conducted at high temperatures under vacuum conditions [31–34].

On the other hand, Saber theoretically estimated the influences of metallic coatings on SKU performance and found that a Mo coating was ideal since it has the relatively close coefficient of thermal expansion with the SKDs and low vapor pressure at high temperature [31]. However, few reports have described the experimental details of the protective coating fabrication and the effectiveness of the coatings on suppressing sublimation of the volatile antimony. In the present work, multilayer thin films (Mo/SiO_x) were

* Corresponding author. Tel.: +86 21 6998 7721; fax: +86 21 6998 7781.
E-mail address: xyhuang@mail.sic.ac.cn (X. Huang).

http://dx.doi.org/10.1016/j.jallcom.2014.03.086
0925-8388/

deposited on the surface of a P-type $Ce_{0.9}Fe_3CoSb_{12}$ SKD via magnetron sputtering.

The effectiveness of the coating films on suppressing the antimony sublimation was examined using an isothermal aging test under vacuum at 823 K, 893 K, and 923 K for various periods by comparison to the uncoated samples. The high temperature stability of the protective coating was evaluated by examination of the inter-diffusion on the coating–SKD boundary. These results show the effectiveness of the Mo/SiO_x multilayer film as a protective coating for the SKD thermoelectric device.

2. Experimental

The P-type SKD $Ce_{0.9}Fe_3CoSb_{12}$ samples were prepared by melting, annealing, and spark plasma sintering (SPS) processes described in our previous publication [35]. Highly pure elements Ce (99.9%, piece), Fe (99.99%, shot), Co (99.95%, shot), and Sb (99.9999%, shot) were chosen as the raw materials. The mixture of the pure metals with the stoichiometric composition was sealed in a quartz tube with carbon depositing on the inner wall. Subsequently, the tube was slowly heated to 1370 K, the temperature was maintained for 12 h. After that, the tube was quenched in a saltwater bath and then annealed at 953 K for 72 h. Finally, the obtained ingot was ground into fine powders by an agate mortar and then sintered by SPS at 850 K for 8 min under a pressure of 60 MPa. The obtained SKD samples were cut into rectangular samples with dimensions of $6 \times 6 \times 2$ mm^3 and then polished using 1-μm diamond paste. Deposition of the Mo and SiO_x thin films was performed in a magnetron sputtering device using 80-mm-diameter Mo and Si targets in the same chamber. The deposition time for both Mo and Si was 30 min. A small of amount of oxygen was introduced during the Si sputtering process to obtain SiO_x. The base pressure of the deposition chamber was kept at 5×10^{-4} Pa.

The coated samples were sealed in an evacuated ampule and then heated to 823 K, 893 K, and 923 K for the isothermal aging test. The aging time was set to 100 h and 250 h for each aging temperature. The phase composition of the samples was analyzed by X-ray diffraction (XRD) using a Rigaku RINT 2000 V (Rigaku, Tokyo, Japan), the microstructure of the sample surface and cross-section was observed by scanning electron microscopy (SEM; JSM-6700F; JEOL, Tokyo, Japan), and the chemical composition was examined by electron probe micro-analysis (EPMA; model 8705QH2; JEOL, Tokyo, Japan) using an energy dispersive spectroscopy (EDS) system.

3. Results and discussion

3.1. Structural and compositional evolutions of Mo/SiO_x multilayer films

Fig. 1 shows typical SEM images of the as-deposited Mo/SiO_x multilayer film on the $Ce_{0.9}Fe_3CoSb_{12}$ bulk sample. The dense array of the Mo/SiO_x film completely covered the SKD substrate without any visible cracks or pin-holes. The Mo and SiO_x layers featured good adhesion without obvious defects or cracks at the boundary. The Mo and SiO_x layers were 2 μm and <1 μm, respectively.

Fig. 2 shows the XRD pattern of the as-prepared Mo/SiO_x film on the $Ce_{0.9}Fe_3CoSb_{12}$ bulk. In addition to the diffraction peaks of the SKD substrate, only that of Mo in the (1 1 0) preferred direction was observed as the main crystal phase of the coating layer. No

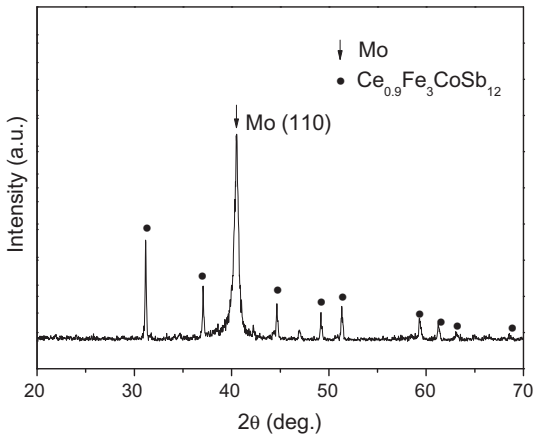

Fig. 2. XRD patterns of the as-prepared SKD/Mo/SiO_x bulk sample.

diffraction peaks corresponding to the SiO_x phase were clearly observed by XRD, indicating that the SiO_x sublayer was amorphous.

Fig. 3 shows SEM images of the Mo/SiO_x surface after aging at the different temperatures for the different time periods. No cracks were observed on the surfaces even after the aging test, implying that the multilayer film adhered well to the SKD substrate material even after long-term and high-temperature treatment.

Fig. 4 shows the cross-sectional microstructure of the samples after aging at the different conditions. Similar to the surface observation, the cross-sectional observation also revealed that both the coated layer and the SKD bulk were free of cracks and pores and showed excellent adhesions between the coating and SKD bulk. However, when we focused on the layer structure and thickness, we found what appeared to be a new layer between Mo and SKD that had formed during the thermal aging process.

The thickness of the newly formed inter-reaction layer increased and that of the Mo layer decreased as aging temperature or period increased. The thickness of the inter-reaction layer was 3 μm after aging at 823 K for 100 h and increased to approximately 6 μm when the aging temperature increased to 923 K. The thickness of the inter-reaction layer changed from 4 μm to 5 μm when the aging period was increased from 100 h to 250 h at 893 K.

To determine the chemical composition of the interlayer formed during aging at high temperatures, EPMA line analysis was used to examine the composition profile along the thickness direction of the multilayer film. Figs. 5 and 6 show the cross-sectional microstructure and concentration profiles of the main elements across the coating after aging for 100 h at 823 K and 923 K, respectively. The Sb partly diffused into the Mo layer, while the Mo diffused toward the SKD bulk to form the interlayer. No Sb was detected in the outer SiO_x layer.

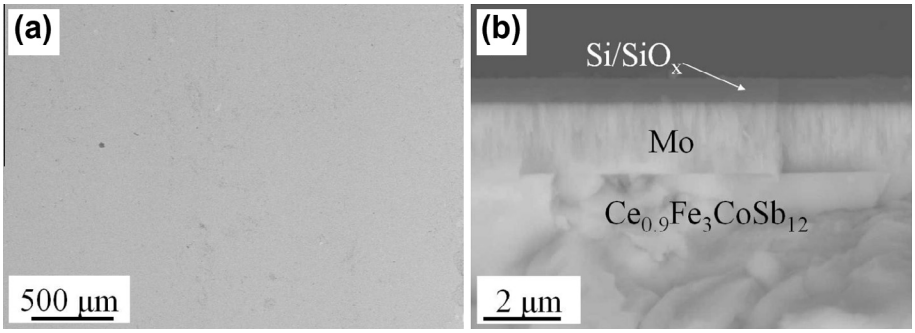

Fig. 1. SEM images of the as-deposited Mo/SiO_x multilayer film on the $Ce_{0.9}Fe_3CoSb_{12}$ bulk sample (a) surface and (b) cross-section.

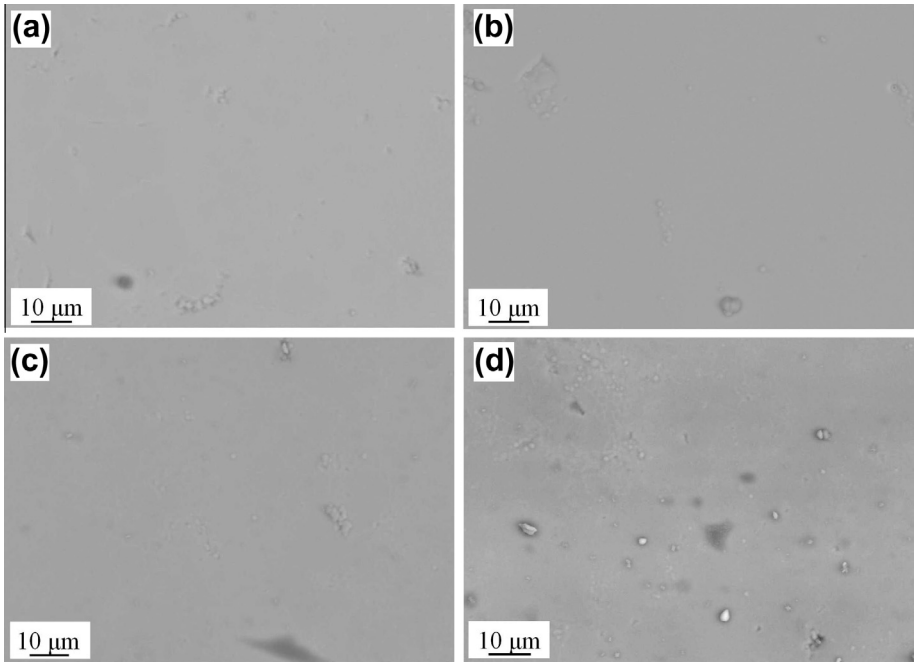

Fig. 3. SEM images of the surface morphology of Mo/SiO_x on SKD aged at (a) 823 K for 100 h, (b) 893 K for 100 h, (c) 893 K for 250 h and (d) 923 K for 100 h.

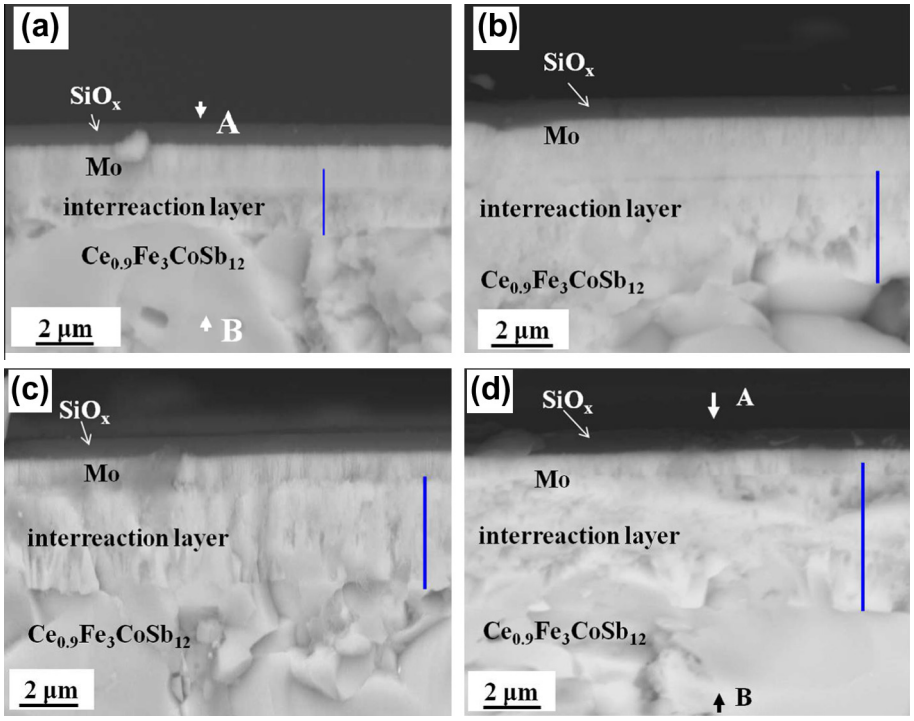

Fig. 4. SEM images of cross-sectional microstructure of SKD/Mo/SiO_x aged at (a) 823 K for 100 h, (b) 893 K for 100 h, (c) 893 K for 250 h and (d) 923 K for 100 h. The bars indicate the thickness of the newly formed interreaction layers after thermal aging.

The coating typically involves three layers: the outermost layer (position 1) is Si with little O content; the intermediate layer (position 2) is Mo with negligible Si content; and the inner layer (position 3) contains Mo and Sb in a 3:7 atomic ratio. Compared to the sample aged at 823 K for 100 h, the inner diffusion layer (position 3) in the sample aged at 923 K for the same period became thicker. In both cases, the inter-reaction layer was dense and stable. More importantly, the Sb diffusion did not penetrate the Mo/SO_x films even after thermal aging at temperatures as high as 923 K for 100 h, implying that the interlayer can block or delay the further diffusion of Sb and Mo. In addition, interlayer formation is believed to be beneficial for increasing adhesion between the SKD and the Mo/SiO_x film.

Fig. 7 compares the XRD patterns of the as-prepared SKD/Mo/SiO_x and those after aging under the different conditions. For the as-prepared Mo/SiO_x multilayer films, $Ce_{0.9}Fe_3CoSb_{12}$ and

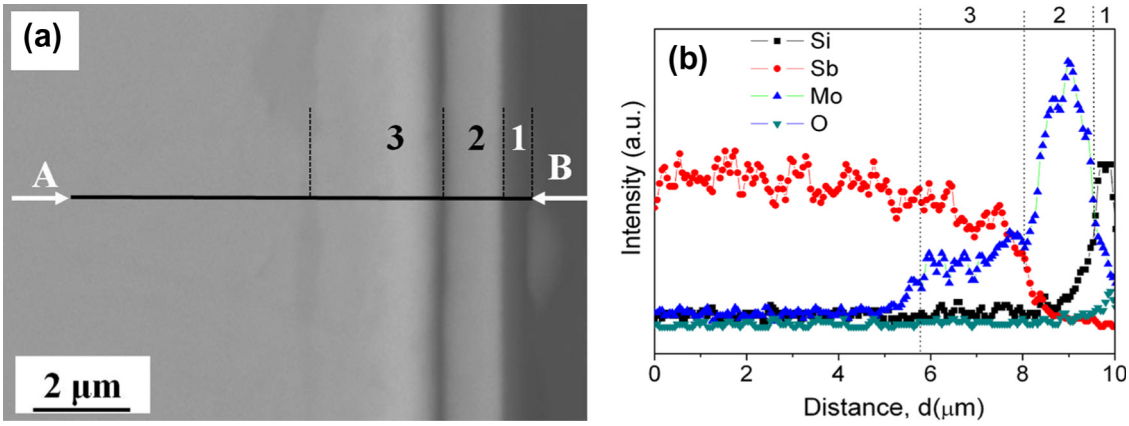

Fig. 5. (a) SEM image of cross-sectional microstructure and (b) concentration profiles of main elements in the multilayer coating aged at 823 K for 100 h.

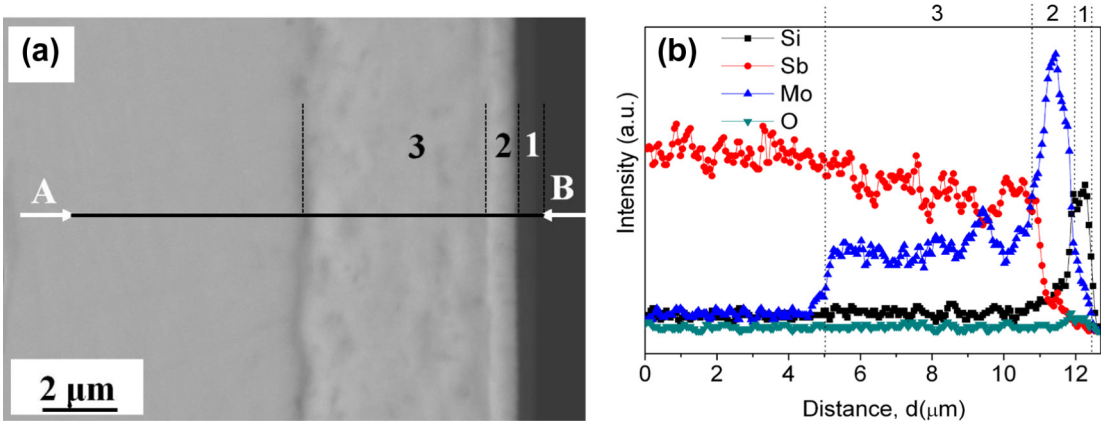

Fig. 6. (a) SEM image of cross-sectional microstructure and (b) concentration profiles of main elements in the multilayer coating aged at 923 K for 100 h.

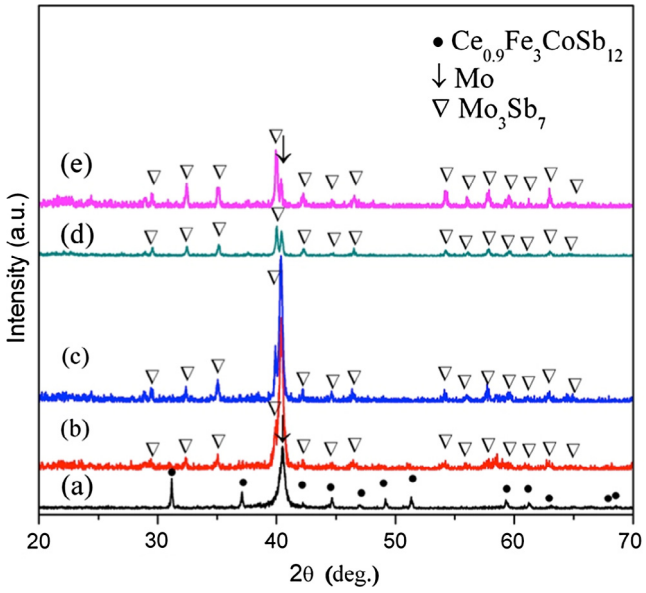

Fig. 7. XRD patterns of (a) the as-prepared SKD/Mo/SiO_x, and the samples aged at (b) 823 K for 100 h, (c) 893 K for 100 h, (d) 893 K for 250 h and (e) 923 K for 100 h.

Mo(110) peaks were clearly observed (Fig. 7a). After the thermal aging process, the SKD diffraction peaks disappeared (Fig. 7b–e) and a series of new diffraction peaks appeared. These new diffraction peaks could be indexed as the Mo_3Sb_7 compound.

Taking into account the SEM observation and EPMA results shown in Figs. 4–6, it is easy to conclude that the interdiffusion of Sb and Mo occurred at high temperature, leading to the formation of the new Mo_3Sb_7 layer due to the Mo/Sb inter-reaction. A phase diagram of the Mo–Sb system also provides the possibility of Mo_3Sb_7 formation at high temperature [36]. Since the Mo phase equilibrates with Mo_3Sb_7, the Mo layer deposited on $Ce_{0.9}Fe_3CoSb_{12}$ changed from Mo/Mo(Sb) to Mo/Mo_3Sb_7 due to the Sb and Mo interdiffusion and reaction. Simultaneously, there seemed to be no difference in the profiles around the Mo/SiO_x (SKD/Mo/SiO_x) interface before and after aging.

There are no characteristic diffraction peaks in the SiO_x sublayer, indicating that the SiO_x film remains amorphous after annealing at the present aging conditions. At the same time, the peaks of the Mo_3Sb_7 layer increase with increasing aging temperature or period (Fig. 7b–e). The Mo_3Sb_7 peaks become stronger and more obvious than the Mo peaks after aging at 893 K for 250 h. The Mo peaks after aging at 823 K and 893 K for 100 h become stronger than those in the as-prepared samples as the degree of Mo crystallization increases. The Mo peaks decrease after aging at 893 K for 250 h and at 923 K for 100 h due to further Mo and Sb reactions. The Mo diffraction peaks are still observable even after being aged at 923 K for 100 h, implying that diffusion slows after Mo_3Sb_7 formation.

3.2. Sb sublimation during aging

The effect of the Mo/SiO_x multilayer film on suppressing Sb sublimation was investigated by comparison of the cross-sectional

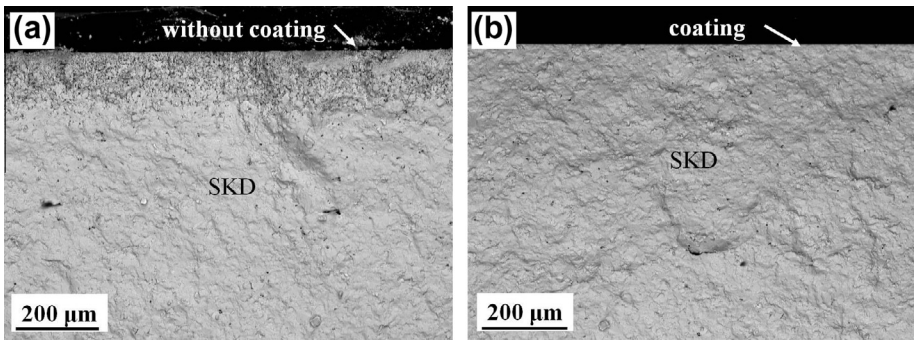

Fig. 8. Cross-sectional microstructure of samples without coating (a) and with Mo/SiO_x coating (b) aged at 923 K for 100 h.

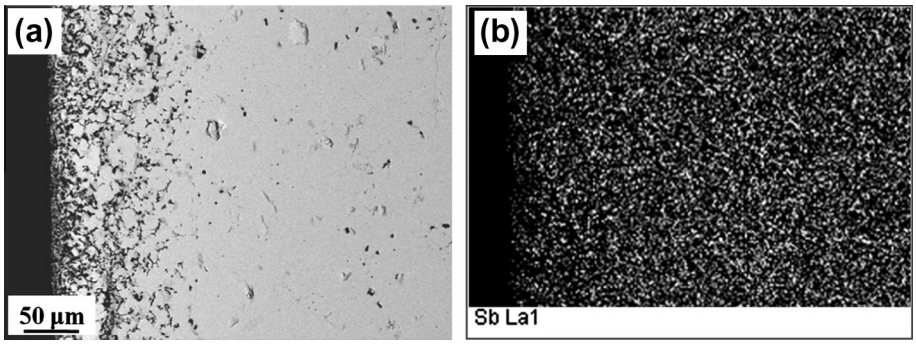

Fig. 9. SEM image and EDX mapping of cross section of uncoated $Ce_{0.9}Fe_3CoSb_{12}$ aged at 923 K for 100 h: (a) SEM micrograph and (b) Sb EDX mapping.

microstructure and Sb distribution of the SKD samples with and without the coating. Fig. 8 shows the cross-sectional SEM images of the SKD samples with and without the coating after aging at 923 K for 100 h. In the uncoated sample, after heat treatment at 923 K for 100 h, evident changes in the microstructural features were observed. The surface portion became porous after heat treatment, and the porosity gradually decreased from the surface portion to the inner portion. The thickness of the porous "layer" was approximately 200 μm for the samples aged at 923 K. On the other hand, no evident change in microstructure was observed in the Mo/SiO_x-coated sample in which there were no visible pores near the coated surface.

To examine the changes in the chemical composition of the samples after heat treatment, energy-dispersive X-ray diffraction

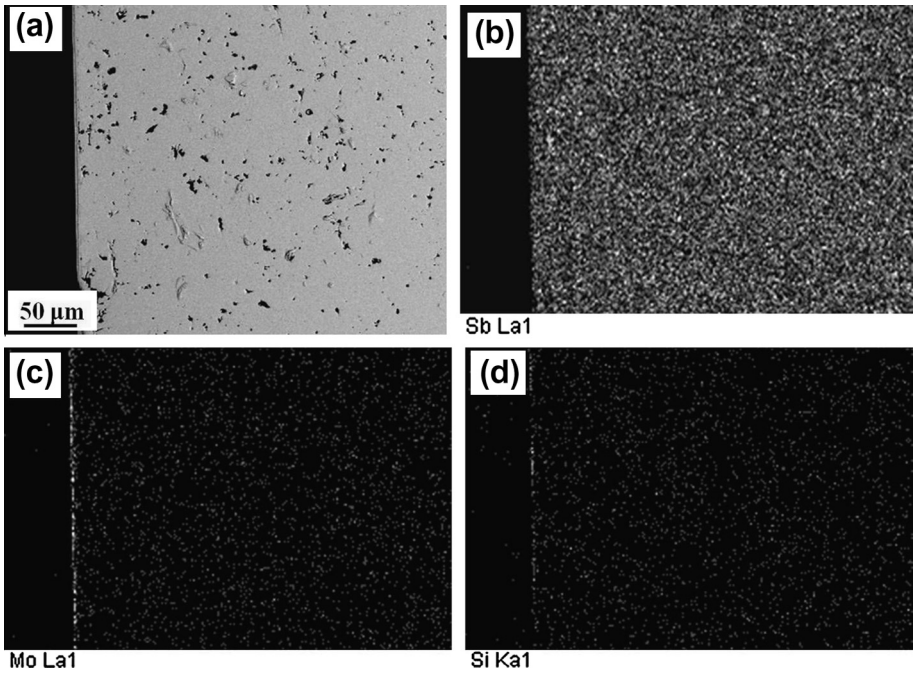

Fig. 10. SEM image and EDX mapping of cross section of SKD/Mo/SiO_x after being aged at 923 K for 100 h: (a) SEM micrograph; (b) Sb EDX mapping; (c) Mo EDX mapping and (d) Si EDX mapping.

(EDX) mapping, including Sb, Fe, Co, Ce, Mo, and Si, was applied to examine the composition profile of the sample cross-sections. The mapping results (not shown here) indicate that even for the uncoated samples, there was no evident difference in Fe, Co, or Ce between the surface and inner portions after heat treatment. Fig. 9 shows that the content of the Sb element increased in the direction from the surface portion to the inner portion for the uncoated samples aged at 923 K for 100 h. Some defects and non-uniformities of the Sb were also observed near the surface. Furthermore, when the SEM microstructure was combined with the Sb distribution, areas with deficient Sb in the EPMA mapping corresponded to those portions with defects or pores in the SEM images. Therefore, the non-uniform distribution of Sb implied that the pores and microstructural defects observed on the SEM image were due to decomposition and Sb sublimation.

Fig. 10 shows the distribution of Sb, Mo, and Si by EDX mapping of a typical cross-sectional area close to the surface of the sample with the Mo/SiO_x coating after aging at 923 K for 100 h. The Sb distribution is uniform throughout the observed area without a visible difference between the surface and inner portions. The existence of the Si- and Mo-containing layers is clearly reflected by the concentrated Si and Mo belt-shaped area on the EDX mapping. The sharp boundaries of the Si- and Mo-containing layers indicate that the Mo and Si on the coated surface are stable at high temperatures without obvious diffusion. These results suggest that the SiO_x/Mo/Mo_3Sb_7 multilayer coating on the $Ce_{0.9}Fe_3CoSb_{12}$ formed by sputtering and diffusion shows excellent chemical stability at high temperatures and acts as an effective protective coating to suppress Sb sublimation at high temperatures.

4. Conclusions

The multilayer Mo/SiO_x film was coated on the $Ce_{0.9}Fe_3CoSb_{12}$ surface by magnetron sputtering. The Mo/SiO_x multilayer film is mainly composed of the stacking of body-centered cubic Mo(1 1 0) and amorphous SiO_x. The interdiffusion of Mo and Sb on the boundary at high temperature resulted in the formation of a Mo_3Sb_7 layer that is stable at high temperature, facilitates adhesion improvements between the SKD and the Mo/SiO_x, and blocks further interdiffusion on the boundary. The coating structure was virtually unchanged after thermal aging, showing excellent thermal and chemical stability. Neither pores nor structural defects were observed in the coated $Ce_{0.9}Fe_3CoSb_{12}$ samples after thermal aging at 823–923 K. The Sb sublimation of $Ce_{0.9}Fe_3CoSb_{12}$ at high temperatures was greatly suppressed by the Mo/SiO_x/Mo_3Sb_7 multilayer coating.

Acknowledgements

This work was supported by the National Basic Research Program of China (973 program) under Project No. 2013CB632504, the National Natural Science Foundation of China (Contract Nos. 51004096, 51072218, and 51102260), and the International S&T Cooperation Program of China (Project No. 2011DFB60150).

References

[1] G. Chen, M.S. Dresselhaus, G. Dresselhaus, J.P. Fleurial, T. Caillat, Int. Mater. Rev. 48 (2003) 45–66.
[2] S.B. Riffat, X. Ma, Appl. Therm. Eng. 23 (2003) 913–935.
[3] V.L. Kuznetsov, A.E. Kaliazin, D.M. Rowe, J. Mater. Sci. 37 (2002) 2893–2897.
[4] J.L. Cui, X.B. Zhao, W.M. Zhao, Mater. Sci. Eng., B 94 (2002) 223–228.
[5] Z. Chen, M.Y. Lin, G.D. Xu, S. Chen, J.H. Zhang, M.M. Wang, J. Alloys Comp. 588 (2014) 384–387.
[6] S. Baba, H. Sato, L. Huang, A. Uritani, R. Funahashi, J. Akedo, J. Alloys Comp. 589 (2014) 56–60.
[7] Y. Zhou, L.L. Li, Q. Tan, J.F. Li, J. Alloys Comp. 590 (2014) 362–367.
[8] L. H Liu, F. Li, Y. P Wei, N. Chen, S. L Bi, H.M. Qiu, G.H. Cao, Y. Li, J. Alloys Comp. 588 (2014) 271–276.
[9] C.A. Figueirêdo, M.R. Gallas, J.E. Zorzi, C.A. Perottoni, J. Alloys Comp. 598 (2014) 266–271.
[10] T.H. Zou, X.Y. Qin, D. Li, L.L. Li, G.L. Sun, Q.Q. Wang, J. Zhang, H.X. Xin, Y.F. Liu, C.J. Song, J. Alloys Comp. 588 (2014) 568–572.
[11] H. Yamada, H. Katsumata, D. Yuasa, S. Uekusa, M. Ishiyama, H. Souma, I. Azumaya, Phys. Procedia 23 (2012) 13–16.
[12] J.F. Deng, J.Q. Li, R.F. Ye, X.Y. Liu, F.S. Liu, W.Q. Ao, J. Alloys Comp. 585 (2014) 173–177.
[13] S.S. Hu, Z. Wang, W.M. Wu, G.Y. Xu, Procedia. Eng. 27 (2012) 186–192.
[14] A.C. Kallel, G. Roux, C.L. Martin, Mater. Sci. Eng. A 564 (2013) 65–70.
[15] S. Ballikaya, C. Uher, J. Alloys Comp. 585 (2014) 168–172.
[16] L.N. Zhou, P.F. Qiu, C. Uher, X. Shi, L.D. Chen, Intermetallics 32 (2013) 209–213.
[17] X.L. Su, H. Li, Y.G. Yan, G.Y. Wang, H. Chi, X.Y. Zhou, X.F. Tang, Q.J. Zhang, C. Uher, Acta Mater. 60 (2012) 3536–3544.
[18] Ping Wei, Wen-Yu Zhao, Chun-Lei Dong, Xuan Yang, Yu Jian, Qing-Jie Zhang, Acta Mater. 59 (2011) 3244–3254.
[19] X.G. Xia, P.F. Qiu, X. Shi, X.Y. Li, X.Y. Huang, L.D. Chen, J. Electron. Mater. 41 (2012) 2225–2231.
[20] J. Leszczynski, K.T. Wojciechowski, A.L. Malecki, J. Therm. Anal. Calorim. 105 (2011) 211–222.
[21] E. Godlewska, K. Zawadzka, A. Adamczyk, M. Mitoraj, K. Mars, Oxid. Met. 74 (2010) 113–124.
[22] D.G. Zhao, C.W. Tian, Y.T. Liu, C.W. Zhan, L.D. Chen, J. Alloys Comp. 509 (2011) 3166–3171.
[23] D.G. Zhao, C.W. Tian, S.Q. Tang, Y.T. Liu, L.D. Chen, J. Alloys Comp. 504 (2010) 552–558.
[24] R. Hara, S. Inoue, H.T. Kaibe, S. Sano, J. Alloys Comp. 349 (2003) 297–301.
[25] H.L. Dong, X.Y. Li, X.Y. Huang, Y.F. Zhou, W. Jiang, L.D. Chen, Ceram. Int. 39 (2013) 4551–4557.
[26] A. Schock, Design, evolution and verification of the general purpose heat source, in: Proceedings. of 15th Intersociety Energy Conversion Engineering Conference, AIAA Paper No. 809203, 1980, pp. 1032–43.
[27] G. Bennett, J. Lombardo, B. Rick, Power performance of the general-purpose heat source radioisotope thermoelectric generator, in: M.S. El-Genk, M. Hoover (Eds.), Space Nuclear Power Systems.
[28] H.L. Dong, X.Y. Li, Y.S. Tang, J. Zou, X.Y. Huang, Y.F. Zhou, W. Jiang, G.J. Zhang, L.D. Chen, J. Alloys Comp. 527 (2012) 247–251.
[29] T. Caillat, J.P. Fleurial, J. Snyder, A. Zoltan, B. Zoltan, A. Borshchevsky, Development of a high efficiency thermoelectric unicouples for high power generation applications, in: A. Ehrlich (Ed.), Proceedings. of 18th International Conference on Thermoelectrics, IEEE, Piscataway, 1999, pp. 473–476.
[30] T. Caillat, A. Borshchevsky, J. Snyder, J.-P. Fleurial, High efficiency segmented thermoelectric unicouples, in: M.S. El-Genk (Ed.), Proceedings of Space Technology and Applications International Forum, American Institute of Physics, Melville, NY, 2000, pp. 1508–1512.
[31] M.S. El-Genk, H.H. Saber, Performance tests of skutterudites and segmented thermoelectric converters, in: T. Caillat, M.S. El-Genk (Eds.), Proceedings of Space Technology and Applications International Forum, American Institute of Physics, Melville, NY, 2004, pp. 541–552.
[32] M.S. El-Genk MS, H.H. Saber, T. Caillat, J. Sakamoto, Energ. Convers. Manage. 47 (2006) 174–200.
[33] H.H. Saber, M.S. El-Genk, Energ. Convers. Manage. 48 (2007) 1383–1400.
[34] H.H. Saber, M.S. El-Genk, T. Caillat, Energ. Convers. Manage. 48 (2007) 555–567.
[35] R.H. Liu, X.H. Chen, P.F. Qiu, J.F. Liu, J. Yang, X.Y. Huang, L.D. Chen, J. Appl. Phys. 109 (2011). 023719-023719-7.
[36] P. Jenson, A. Kjekskus, T. Skansen, Acta Chem. Scand. 20 (1966) 403–416.